Chemical Engineering Journal 96 (2003) 55–69

Chemical Engineering Journal

www.elsevier.com/locate/cej

Mechanisms of physical and reaction enhancement of mass transfer in a gas inducing stirred slurry reactor

K.C. Ruthiya, J. van der Schaaf, B.F.M. Kuster, J.C. Schouten*

Laboratory of Chemical Reactor Engineering, Department of Chemical Engineering and Chemistry, Eindhoven University of Technology, P.O. Box 513, 5600 MB Eindhoven, The Netherlands

Abstract

This study further evaluates four mechanisms for the enhancement of gas–liquid (G–L) mass transfer [Can. J. Chem. Eng. 81 (2003) 632–639]: (1) boundary layer mixing, (2) shuttling, (3) coalescence inhibition, and (4) boundary layer reaction. The present work focuses on G–L mass transfer enhancement in a gas inducing stirred slurry reactor (GIR) in a range of mixing intensities (0.5–30 kW m_l^{-3}). Physical enhancement (mechanisms 1–3) and reaction enhancement (mechanism 4) are investigated separately by dynamic gas absorption experiments without reaction and pseudo-steady-state gas absorption experiments with reaction. Two Pd-catalysed reactions are studied: oxidation of glucose (aqueous phase) and hydrogenation of α-methyl styrene (AMS) (organic phase). The influence of lyophobic carbon particles, lyophilic silica particles, and of electrolyte on G–L mass transfer is studied. Mechanism 1 is predominant at low mixing intensity, whereas the contribution of mechanism 2 is insignificant. Carbon/silica particles and electrolyte individually increase the volumetric G–L mass transfer coefficient, which is mainly attributed to mechanism 3. Especially a combination of particles and electrolyte strongly increases G–L mass transfer. Mechanism 3 also holds at higher mixing intensity. Mechanism 4 magnifies the impact of mechanisms 1 and 3. The carbon/silica particle lyophobicity strongly influences the interaction with the G–L interface. In aqueous glucose slurry, physical enhancement (mechanisms 1 and 3) and reaction enhancement (mechanism 4) are observed. In organic AMS–cumene slurry, lyophobicity/lyophilicity affects reaction enhancement only.

Keywords: Gas–liquid mass transfer mechanisms; Catalyst particle lyophobicity; Glucose oxidation; α-Methyl styrene hydrogenation; Stirred slurry reactor

1. Introduction

Gas–liquid mass transfer in slurry reactors is a key parameter in commercial three phase systems for, e.g., Fischer–Tropsch synthesis, liquid phase methanol synthesis, or biological waste water treatment. Sharma and Mashelkar [2] first qualitatively demonstrated the increase of the gas absorbtion rate by small gas-absorbing particles in a bubble column. Lee and Tsao [3] confirmed this for a stirred slurry reactor. Kars et al. [4] introduced a shuttle effect to explain this mass transfer enhancement. Alper et al. [5] first quantitatively demonstrated mass transfer enhancement by active carbon particles, showing that the two-film model of Whitman developed in 1923 and the penetration model, developed to explain non-stationary phenomena of mass transfer [6,7], could not describe the observed mass transfer phenomena. More recently, gas–liquid mass transfer enhancement by particles suspended in the liquid phase has been investigated by several authors [5,7–12] and various models/mechanisms have been proposed for describing this enhancement. An important aspect of G–L mass transfer enhancement appears to be the sticking of particles to the G–L interface [9,10,13] and this attachment is termed as particle to bubble adhesion (PBA), schematically shown in Fig. 1. This adhesion is determined by a plethora of parameters, e.g., liquid properties (surface tension, viscosity, density, surface-active components, and nature of liquid, aqueous or organic), particle properties (diameter, lyophobicity, surface roughness, partition coefficient, i.e., adsorption capacity between liquid and solid, and three-phase contact angle), and process parameters (turbulence intensity, particle concentration). In slurry reactors, PBA affects the gas hold-up, the bubble size distribution, and the bubble coalescence rate. In our previous work in a surface aeration reactor with a flat G–L interface [1], four mechanisms of mass transfer enhancement were introduced:

Abbreviations: AMS, α-methyl styrene; C, carbon; E, electrolyte (sodium gluconate in this study); G, glucose; GIR, gas inducing reactor; PBA, particle–bubble adhesion

* Corresponding author. Tel.: +31-40-2472850; fax: +31-40-2446653.
E-mail address: j.c.schouten@tue.nl (J.C. Schouten).
URL: http://www.chem.tue.nl/scr.

1385-8947/$ – see front matter © 2003 Elsevier B.V. All rights reserved.
doi:10.1016/j.cej.2003.08.005

Nomenclature

a_l	surface area per unit volume of (bubble and particle free) liquid ($m^2\ m_l^{-3}$)
a_s	surface area of catalyst per unit volume of (bubble and particle free) liquid ($m^2\ m_l^{-3}$)
C_{cat}	catalyst concentration in the reactor ($g\ l^{-1}$)
C_i	saturated concentration of gas at liquid side of G–L interface ($mol\ m_l^{-3}$)
C_l	gas concentration in bulk liquid ($mol\ m^{-3}$)
C_s	dissolved gas concentration in liquid filled catalyst particles ($mol\ m_c^{-3}$)
C_{sen}	sensor response ($mol\ m^{-3}$)
C^O	saturated concentration of gas at liquid side of G–L interface at 1.1 bar ($mol\ m_l^{-3}$)
d_I	impeller diameter, $d_I = 0.045$ in all experiments (m)
d_p	particle diameter (m)
d_T	reactor diameter (m)
D_e	effective diffusivity ($m^2\ s^{-1}$)
D_m	molecular diffusivity ($m^2\ s^{-1}$)
E_p	physical enhancement factor as defined in Eq. (17) (–)
E_r, E_t	reaction and total enhancement factor as defined in Eq. (18) (–)
FE^{CO}	fraction of active metal Pd at outer surface of catalyst particle (–)
H_a	distance between bottom of reactor and impeller blade (m)
He	Henry coefficient ($Pa\ mol^{-1}\ m^3$)
H_l	liquid height in gas inducing reactor (m)
k_a	adsorption rate constant $= 8.85 \times 10^{-7} \exp(29540.4/RT)$ ($m_c^3\ mol^{-1}$)
k_l	G–L mass transfer coefficient ($m\ s^{-1}$)
$k_{overall}$	overall mass transfer rate defined in the Eq. (11) (s^{-1})
k_r	reaction rate constant ($m^3\ mol_{Pd}^{-1}\ s^{-1}$)
k_s	L–S mass transfer coefficient ($m\ s^{-1}$)
k_{sen}	sensor constant (s^{-1})
k_{sr}	surface reaction rate constant $= 1.29 \times 10^{12} \exp(-54436.4/RT)$ ($mol\ m_c^{-3}\ s^{-1}$)
L_t	weight specific Pd surface atoms calculated as $(\%Pd/M_{Pd})FE^{CO}$ ($mol\ kg_c^{-1}$)
m	partition coefficient ($m_l^3\ m_c^{-3}$)
N	impeller rotation speed (s^{-1})
N_p	impeller power number, taken as 5 from Bates et al. [44] (–)
p	pressure (kPa)
p_{H_2}	H_2 partial pressure (kPa)
p_{O_2}	O_2 partial pressure (kPa)
P	power dissipated by impeller, $P = N_p \rho_l N^3 d_I^5$ (kW)
R_v	observed volumetric reaction rate ($mol\ m^{-3}\ s^{-1}$)
t	time (s)
V_g	total volume of the gas phase in the reactor (m^{-3})
V_l	total volume of the liquid phase in the reactor (m_l^{-3})
w_b	width of baffle in the reactor (m)
x_{AMS}	mole fraction of AMS (–)

Greek letters

δ_l	G–L film thickness at liquid side of interface (m)
η	effectiveness factor (–)
μ_l	liquid viscosity (Pa s)
ρ_l	liquid density ($kg\ m_l^{-3}$)
ρ_p	particle density ($kg_c\ m_c^{-3}$)
σ_l	surface tension of liquid ($N\ m^{-1}$)
τ_p	tortuosity taken as 3.2 from Kawakami et al. [32] (–)

- Mechanism 1: Boundary layer mixing—Four different physical phenomena influence the convective mass transfer and the concentration gradient at the G–L interface: (i) the effective G–L boundary layer thickness is reduced by collisions of the particles with the boundary layer [12,14] which increases the G–L mass transfer coefficient (k_l); (ii) large particles ($d_p > \delta_l$) induce a local degree of turbulence at the G–L interface which increases the refreshment rate of the liquid in the G–L boundary layer by mixing with the bulk liquid. However, particles may also dampen the turbulence at the G–L interface, leading to a decrease of k_l [15]; (iii) one might expect a priori that the k_l depends on the rate of coalescence of gas bubbles for two reasons: (a) bubble coalescence by particles is especially induced at low mixing intensities and it may give rise to larger bubbles that have a more mobile interface (larger k_l)

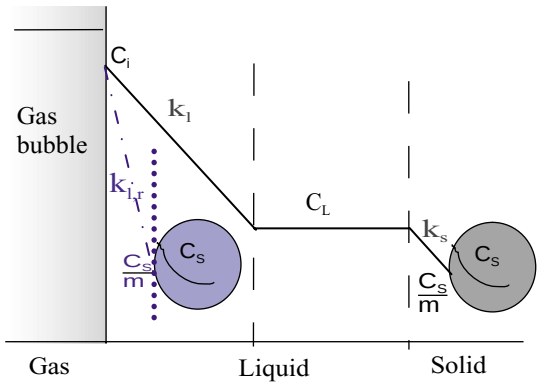

Fig. 1. Schematic representation of mass transfer from gas to liquid to solid in series and direct gas to solid in parallel with particle–bubble adhesion, where both physical and reaction enhancement of mass transfer occurs.

[14,16,17]; (b) bubble coalescence causes re-dispersion of entrained gas, which means additional surface renewal (larger k_l); (iv) small particles ($d_p \leq \delta_l$) may decrease k_l, due to a decrease in the effective volume fraction of the liquid available for diffusion of gas at the interface. The number of particles adhering to bubbles is dependent on the balance between shear stress and adhesion forces. The shear stress is proportional to the stirrer speed in a stirred tank reactor and proportional to the superficial gas velocity in a bubble column. When the shear forces become higher than the adhesion induced forces, particles are removed from the G–L interface. The relative effect of PBA on the increase of the rate of mass transfer will therefore decrease at higher mixing intensities [1].

- Mechanism 2: Shuttling—If the particles have a high specific surface area and porosity, then, in addition to mechanism 1, the particles that penetrate the liquid film at the G–L interface will adsorb some of the dissolved gas. When these particles return to the bulk liquid, they will desorb the adsorbed gas. In this way, transport of the gas to the bulk liquid is increased due to the moving particles. In agitated slurry reactors, an increase of the volumetric G–L mass transfer coefficient ($k_l a_l$), is ascribed to an increase of k_l of about 200–300% [4,5] and 20–50% [18] due to this shuttle effect. Mechanism 2 is dependent on the partition coefficient (m) of the particles and on the residence time of the particles in the G–L boundary layer. This shuttling mechanism has been modelled using the penetration theory [7,19] and it was concluded that only for a very high adsorption capacity of particles ($m \geq 400$), mechanism 2 becomes important. Vinke et al. [13] showed an enhancement of mass transfer for small lyophobic particles with a partition coefficient of $m = 100$–300. However, in the same study, experiments with other type of lyophilic particles showed no such enhancement despite their large partition coefficient ($m = 800$–2500). Mechanism 2 is predominant in case of particles of size equal or smaller than the G–L boundary layer (typically 5 μm), if a significant number of particles is present at the interface. The coverage of the bubble surface by these particles does not result in a partial blocking of the interfacial area for mass transfer as found for particles with larger size (100–200 μm) and for non-wettable particles [17,20]. Therefore, it is expected by mechanism 2 that increasing the particle concentration and with increasing mixing intensity, the visiting frequency of particles at the G–L interface will increase, leading to an increased transport of gas from the G–L interface to the bulk liquid, which will result in a larger value of k_l.

- Mechanism 3: Coalescence inhibition—Particles adhering to the gas bubbles and electrolyte in the slurry can reduce or hinder coalescence of gas bubbles. This increases the value of the G–L interfacial area a_l and therefore the volumetric mass transfer coefficient ($k_l a_l$). The five different (groups of) physical properties of influence to mechanism 3 are: (i) surface tension of liquid; (ii) viscosity and density of liquid/slurry; (iii) ionic forces; (iv) lyophobicity of particles (wettability); (v) particle size. Lindner et al. [8] have measured a gas hold-up increase of approximately 300% due to an electrolyte (salt solution) caused by a decreased bubble coalescence rate in both a stirred reactor and a bubble column. Kluytmans et al. [14] also found an increase of the bubble interfacial area in a slurry bubble column. Marrucci [21] and Prince and Blanch [22] conclude that due to ionic forces or the local electrostatic potential at the G–L interface, the film drainage speed between two approaching bubbles is slowed down, resulting in a lower rate of bubble coalescence and an increased number of smaller bubbles. Schumpe et al. [20] found for bubble columns that small carbon particles have a coalescence hindering effect on very small “ionic” bubble clouds. Jamialahmadi and Muller-Steinhagen [23] demonstrated that wettable particles tend to repel the gas interface, therefore acting as a buffer between two adjacent gas bubbles. This stabilises small bubbles and therefore the formation of large bubbles by coalescence is delayed. The opposite effect is found for non-wettable particles (using polypropylene). However, Quicker et al. [24] found contradictory results (a_l is constant) and attributed the increase in k_l to the shuttling of particles. With increasing superficial gas velocity or stirrer speed, the shear stresses in the system increase, decreasing the effect of electrolyte and solid particles on the increase of the G–L interfacial area [14].

- Mechanism 4: Boundary layer reaction or grazing effect—When small particles catalyse a chemical reaction at the G–L interface, significant conversion occurs within the diffusion layer around the gas bubbles, thereby increasing the rate of mass transfer. As the concentration of gaseous reactants in the film layer is higher than in the bulk liquid, the reaction rate in the film layer will be higher. Mass transfer enhancement during reaction is a function of the lyophobicity and activity of the catalyst particles, and of the turbulence intensity in the reactor [1,8,12]. Mechanism 4 can further enhance the effect of mechanisms 1 and 3.

Though much research has already been documented on G–L mass transfer enhancement, knowledge of the exact mechanism of increase in either the G–L mass transfer coefficient, k_l (physically by mechanisms 1 and 2), or the G–L interfacial area, a_l (mechanism 3), or enhancement due to chemical reaction (mechanism 4) is still rudimentary [7,12,17,25,26]. Also, no literature is available on mass transfer enhancement for hydrogen gas in organic liquids, although hydrogenation reactions in slurry systems comprise an important class of chemical reactions. Therefore, the objective of this work is to further clarify which mechanisms lead to the observed increase of the rate of G–L mass transfer.

2. Experimental procedure and data treatment

Dynamic gas absorption and pseudo-steady-state absorption experiments with and without reaction are performed in a gas inducing stirred slurry reactor (GIR). Mass transfer enhancement is investigated as a function of the following parameters: particle material (carbon and silica); organic and aqueous liquid; electrolyte concentration; chemical reaction; and mixing intensity. Oxidation of glucose (aqueous phase) and hydrogenation of α-methyl styrene (AMS) (organic phase) are chosen as model reactions. Both reactions are catalysed by Pd supported on carbon and silica particles. The corresponding experimental set-ups are schematically shown in Fig. 2a and b. The gas inducing reactor is a double walled glass reactor with a total volume of 1 l, equipped with four symmetrically placed, equal sized baffles and a hollow four-bladed gas-inducing impeller. Gas is sucked in through the impeller, creating gas bubbles in the liquid. Prior to each experiment, carbon and silica particles were cleaned from organic contaminants and consecutively dried and stored at 363 K. To make sure that all particles are completely wetted at the start of each experiment, the particles were mixed with liquid for 1 h preceding each experiment. Information about the experimental conditions is given in Table 1. The surface tension of the liquid is measured with a digital Tensiometer K10T. The viscosity of the liquid is measured with a Rheometer AR 1000 N. The properties of the catalyst particles are given in Table 2. The heat of immersion, ΔH_i, is a measure of the degree of lyophobicity of the particles and ranges between 0 and $-355\,\mathrm{mJ\,m^{-2}}$ [9,10,13]. Therefore, the carbon particles are more lyophobic than the silica particles, see Table 2. Both chemical reactions are carried out under mass transfer limiting conditions in order to properly assess mass transfer enhancement and the effects related to particle to bubble adhesion.

Table 1
Characteristics of the reactor, experimental conditions and physical constants used in this study

Symbol	GIR, H_2	GIR, O_2
H_a/H_l	0.30	0.40
d_l/d_T	0.46	0.46
w_b/d_T	0.10	0.13
H_l/d_T	1.00	0.74
T (K)	303	323
P (kPa)	103–109	103.33
V_l (m^3)	0.5×10^{-3}	0.5×10^{-3}
V_g[a] (m^3)	0.899×10^{-3}	0.635×10^{-3}
C_{gluc} (mol m^{-3})	–	500
C_{AMS}[b] (mol m^{-3})	6152	–
He_{H_2}[c] (kPa mol^{-1} m^3)	34.112	–
He_{O_2}[d] (kPa mol^{-1} m^3)	–	108.32
D_{m,O_2}[e] ($m^2\,s^{-1}$)	–	2.755×10^{-9}
D_{m,H_2}[f] ($m^2\,s^{-1}$)	1.252×10^{-8}	–
No. of experiments (without reaction)[g]	95	312
No. of experiments (with reaction)	48	40

[a] Calculated from pressure sensor and known values of gas flow rate.
[b] 81.05 mol%, 80 vol.%, cumene is used as a solvent.
[c] $He = x_{AMS} \times 4450 \exp(628/T) + (1 - x_{AMS}) \times 4060 \exp(597/T)$; [45].
[d] $He^{-1} = 0.54342 \exp[-66.7354 + 8747.55/T + 24.4526 \ln(T/100)]$; [46].
[e] Wilke–Change correlation [46], $D_{m,O_2} = 6.85 \times 10^{-15} T \mu_l^{-1}$, where $\mu_l(T) = -2 \times 10^{-5}(T - 273.15) + 0.0018$; fitted from [47] for 0.5 M glucose solution.
[f] $D_{m,H_2} = (294.64 - 48.632 x_{AMS}) \times 10^{-8} \exp(-13.4 \times 10^3/RT)$; fitted from [34].
[g] Distilled water (22), carbon–water (40), electrolyte–water (108), electrolyte–carbon–water (100), silica–AMS (34), carbon–AMS (61), silica–water (18), glucose–electrolyte (24).

Table 2
Physical properties of the catalyst and supports used during oxidation and hydrogenation reactions[a]

Code	G-4781	Q500-191	Q500-130	42864
Pd (wt.%)	–	3	–	3
Support	SiO_2	SiO_2	Carbon	Carbon
Distribution	–	Uniform	–	Eggshell
d_p[b] (μm)	64	44	30	40
d_p distribution[b]	–	–	7, 27, 78	2.5, 24, 100
S_{BET}[c] ($m^2\,g^{-1}$)	514	278	1108	850
$V_{s,p}$[d] (ml g^{-1})	1.63	2.08	1.60	1.19
ϵ_p[d]	0.8515	0.88	0.65	0.6614
FE^{CO}[e] (%)	–	39.26	–	16.79
L_t (mol kg_c^{-1})	–	0.1107	–	0.0473
ΔH_i[f] (mJ m^{-2})	−201	−228	−54	−70

[a] Supplied by Engelhard B.V. and Promeks ASA. Carbon samples have 50 ± 3 wt.% moisture.
[b] Measured using Coulter counter LS 130 in aqueous suspension. Particle size distribution 5% < 2.5 μm, 50% < 24 μm, 100% < 100 μm. Same % of distribution holds for other samples.
[c] Measured using N_2 physisorption in ASAP-equipment from Micromeritics.
[d] Measured using mercury porosimetry in Micromeritics Autopore IV 9500, $\epsilon_p = V_{s,p}\rho_s/(1 + V_{s,p}\rho_s)$ and verified using $\rho_s = \rho_{pg}/(1 - \epsilon_p)$; $\rho_{pg} = 450 \pm 50$ (kg m^{-3}), $\Delta\rho \approx 90$ for carbon and 300 for silica particles.
[e] Fraction exposed: measured using CO chemisorption in modified ASAP-equipment.
[f] Heat of immersion in water by microcalorimetry.

2.1. Aqueous phase: glucose solution and electrolyte

Experiments were carried out with distilled water, slurries with carbon or silica particles, electrolyte (sodium gluconate), and slurries with combinations of carbon or silica particles and electrolyte. A mixture of nitrogen and oxygen ($p_{O_2} = 0.2$ bar) is continuously fed to the reactor, where the oxygen reacts with the glucose. Because the supported Pd–Bi catalyst is poisoned by the reaction product gluconic acid, the pH is controlled (at a value of 9) to maintain a constant high reaction rate. This is done by adding 5 M NaOH solution online from a burette, which is a measure of the reaction rate. The temperature is maintained at 323 K. The liquid phase oxygen concentration during the reaction is monitored using an Ingold electrochemical oxygen sensor, to corroborate mass transfer limiting conditions, viz., $C_{l,O_2} \approx 0\,\mathrm{mol\,m_l^{-3}}$. The stirring rate and the electrolyte concentration are varied at each particle loading for each type of slurry.

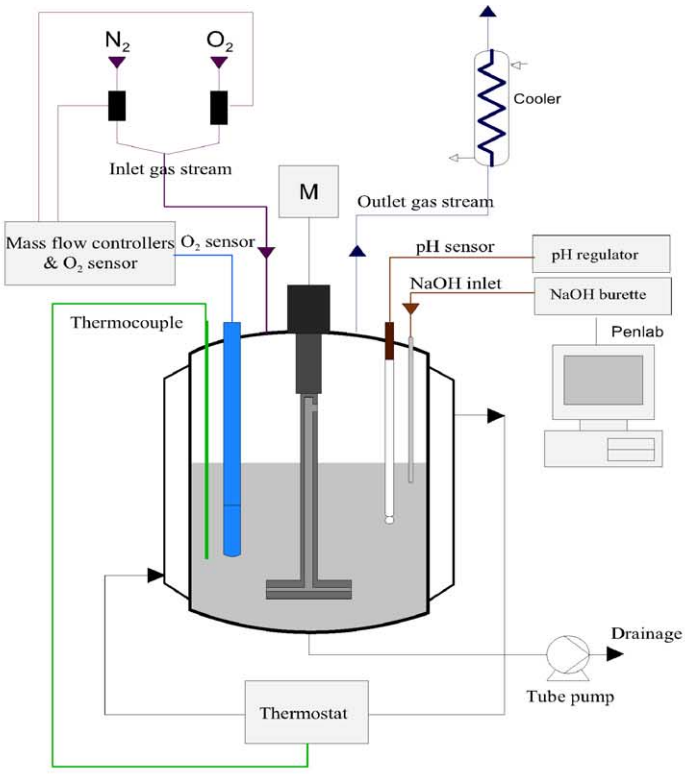

(a) GIR, Oxidation

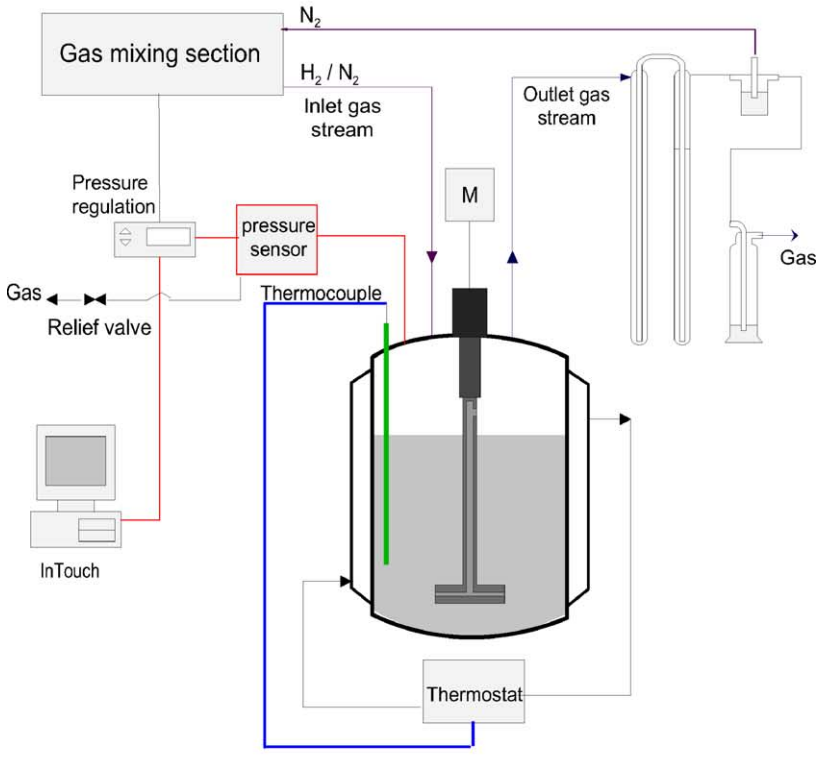

(b) GIR, Hydrogenation

Fig. 2. Schematic diagram of the experimental set up (a) used for dynamic gas absorption with saturation and pressure step method, and pseudo-steady-state glucose oxidation to gluconic acid and (b) used for dynamic gas absorption as well as pseudo-steady-state absorption for hydrogenation of AMS to cumene.

2.2. Organic phase: AMS and cumene

Experiments were carried out with AMS–cumene (80:20 vol.%) slurries with carbon or silica particles and supported Pd catalysts. The pressure in the reactor is controlled using an electronic differential pressure transmitter. The system is degassed completely with a vacuum pump everytime before starting the experiments. The reaction temperature is maintained at 303 K. The stirring rate is varied at each particle loading for each type of slurry. The initial specific rate of absorption of hydrogen is determined from the recorded pressure vs. time curve for that run until no significant change in the gas pressure is indicated by the pressure sensor. The rate of reaction is determined from the dynamic pressure change by hydrogen gas absorption. The stirring rate is varied at each particle loading for each type of slurry.

2.3. Pressure-step method and saturation method without reaction

The physical G–L mass transfer coefficient of oxygen absorption in the glucose solution is measured using both the pressure-step method [27,28] and the saturation method (discontinuous switch from nitrogen to oxygen under exact flow conditions). In both methods, the two-film model describes the rate of mass transfer. The liquid side mass transfer is represented by $k_l a_l$ and, in most cases, determines the overall rate of gas–liquid mass transfer, while the gas side mass transfer resistance is negligible. When using the pressure-step method, the slurry is stripped by nitrogen until the dissolved-oxygen concentration is almost nil. Then the nitrogen flow is shut down until all bubbles have escaped from the water. Subsequently, the liquid bulk is saturated with 0.1 bar oxygen over-pressure. When an equilibrium concentration is established, the pressure in the reactor is instantaneously decreased to the original operating pressure by pinching of the gas-outlet valve. It is assumed that the liquid and the gas are perfectly mixed. Therefore, the dissolved-oxygen concentration is given by

$$\frac{dC_l(t)}{dt} = k_l a_l (C_i - C_l(t)) \tag{1}$$

The boundary condition is: $C_l = C^0$ at $t = 0$ (saturation concentration at 1.1 bar oxygen elevated pressure). The volumetric mass transfer coefficient $k_l a_l$ is determined by a least square fit of Eq. (1) to the experimentally obtained values of $C_l(t)$ measured with the oxygen sensor. The sensor response to a change in oxygen concentration has a finite delay, which is described by a first-order process. This delay in the response is of the order of magnitude of the time constant of the gas–liquid mass transfer. Therefore, the sensor response time should be incorporated in the overall mass transfer model. Eq. (2) represents the first-order response of the oxygen sensor:

$$\frac{dC_{sen}(t)}{dt} = k_{sen}(C_{sen}(t) - C_l) \tag{2}$$

The sensor constant, k_{sen}, is a function of the degree of turbulence at the membrane surface and it changes as a function of stirring intensity, electrolyte concentration, and carbon or silica particle concentration. Sensor constants were estimated using the saturation method three times and values in the range of 0.08–0.2 s^{-1} (±5% error) were calculated. The values of the sensor constant were then combined with Eq. (1), resulting in Eq. (3):

$$C_{sen}(t) = C_i - \frac{C_i - C^0}{k_{sen} - k_l a_l}[k_{sen}\, e^{-k_l a_l t} - k_l a_l\, e^{-k_{sen} t}] \tag{3}$$

The G–L mass transfer coefficient, $k_l a_l$, was then determined from non-linear multiple regression of $C_{sen}(t)$ against time t, by the Levenberg–Marquardt method. The value of $k_l a_l$ is calculated using the pressure step method twice and values in the range of 0.02–0.36 s^{-1} (±3% error) were calculated.

2.4. Dynamic gas absorption method without reaction

The physical G–L mass transfer coefficient of H_2 absorption in an organic AMS–cumene mixture is determined with the dynamic gas absorption method. This method is based on the dynamic pressure change by H_2 gas absorption. The mass balance for a gas dissolving in an (ideally mixed) liquid phase, can be written as

$$\frac{-V_g}{V_l RT}\frac{dp}{dt} = (k_l a_l)_p \left(\frac{p}{He} - C_l\right) \tag{4}$$

with

$$C_l = \frac{V_g}{V_l RT}(p_0 - p) \tag{5}$$

The Henry coefficient, He, is determined at equilibrium where dp/dt is zero and the pressure equals the equilibrium pressure p_{eq}. Substituting this in the equation above gives

$$He = \frac{p_{eq}}{C_i(t = \infty)} = \frac{V_l RT}{V_g}\frac{p_{eq}}{p_0 - p_{eq}} \tag{6}$$

Substituting Eq. (5) and solving the differential equation (4) from initial time $t = 0$, pressure $p = p_0$, to time t, and pressure p, gives

$$(k_l a_l)_p = \frac{1}{t}\frac{Q}{Q+1}\ln\left(\frac{p_0}{(Q+1)p - Qp_0}\right), \quad Q = \frac{V_g He}{V_l RT} \tag{7}$$

The value of the 'pure' volumetric G–L mass transfer coefficient, $(k_l a_l)_0$, is determined from a similar procedure in the absence of particles and electrolyte. All the experiments are done three times and the maximum standard deviation is 2%.

2.5. Pseudo-steady-state absorption with reaction

The oxidation reaction is carried out with carbon or silica supported Pd–Bi catalyst, and selectively produces gluconic acid. The hydrogenation reaction is carried out with carbon or silica supported Pd catalyst, and selectively produces cumene. Under the operating conditions used, the reaction at the catalytic site is first order in oxygen and in hydrogen concentration due to G–L mass transfer limitations and zero order in glucose concentration [30] and in AMS concentration [29]. Neglecting mass transfer in the gas phase, and assuming an ideally mixed gas and liquid phase with reaction only in the bulk liquid (right side of Fig. 1), the following equations describe the volumetric reaction rate, R_v:

$$R_v = (k_l a_l)_r (C_i - C_l) \tag{8}$$

$$R_v = k_s \frac{6C_{cat}}{d_p \rho_p} \left(C_l - \frac{C_s}{m} \right) \tag{9}$$

$$R_v = \eta k_r L_t C_{cat} C_s \tag{10}$$

Eliminating C_l and C_s from the above equations results in the following equation for the reaction rate:

$$k_{overall} = \frac{R_v}{C_i} = \left[\frac{1}{(k_l a_l)_r} + \left(\frac{d_p \rho_p}{6k_s} + \frac{1}{\eta m k_r L_t} \right) \frac{1}{C_{cat}} \right]^{-1} \tag{11}$$

where

$$C_{i,O_2} = \frac{p_{O_2}}{He_{O_2}}, \qquad C_{i,H_2} = \frac{p_{H_2}}{He_{H_2}} \tag{12}$$

$k_{overall}$ is a rate constant for the total rate of reaction and can be calculated with linear regression from the volumetric reaction rate, R_v, against the equilibrium G–L interfacial concentration C_i, at a specific partial pressure. The equations for the catalyst effectiveness factor, η, and the Thiele modulus, ϕ, for the uniform catalyst and first-order reaction are given by [31]. The intrinsic reaction rate coefficient for the hydrogenation reaction, k_r, has been derived on the basis of Langmuir–Hinshelwood mechanisms, and is calculated from [32,33],

$$k_r = \frac{k_{sr} k_a}{(1 + \sqrt{k_a C_s})^2} \frac{1}{(L_t \rho_p)_{lit}} \tag{13}$$

where Arrhenius-type equations for the surface reaction rate coefficient, k_{sr}, and the hydrogen adsorption equilibrium coefficient, k_a, are given in the Nomenclature. The literature value of $(L_t \rho_p)_{lit}$ is 7.38 mol/m$_c^3$, assuming the dispersion of active metal of 20% for the catalyst used by [32,33], which was verified with the data obtained from [30,34,35]. The value of k_r for oxidation under mass transfer limiting conditions is 22 m^3 mol$_{Pd}$ s^{-1} at 323 K [36] and for hydrogenation a value of 3.13 m^3 mol$_{Pd}$ s^{-1} at 303 K is obtained from Eq. (13) for C_s up to 3.16 mol m$_c^{-3}$. To estimate the limitations set by liquid–solid mass transfer, the Sherwood–Frössling correlation for k_s [37] is used:

$$Sh = 2 + 0.4\, Re^{1/4}\, Sc^{1/3} \tag{14}$$

$$Sh = \frac{k_s d_p}{D_m}, \quad Re = \frac{N_p d_I^5 N_I^3 d_p^4 \rho_l^3}{V_l \mu_l^3}, \quad Sc = \frac{\mu_l}{\rho_l D_m} \tag{15}$$

where Sh, Re, and Sc are the Sherwood, Reynolds, and Schmidt number, respectively. For the aqueous slurry, Re = 0.5–55 (400–1500 rpm) with corresponding Sh = 3.5–8.5. For the organic slurry, Re = 0.9–1090 with corresponding Sh = 4–9.7. For the hydrogenation reaction, Eq. (11) is solved by assuming m = 1, k_s given by Eq. (14) and k_r given by Eq. (13). For the oxidation reaction, the liquid phase concentration of oxygen is zero during the reaction. Therefore, the overall rate equation is given by

$$k_{overall,O_2} = \frac{R_v}{C_{i,O_2}} = (k_l a_l)_r \tag{16}$$

The reaction enhancement factor can then be calculated with the obtained values of $(k_l a_l)_r$.

2.6. Definition of physical enhancement and reaction enhancement

The physical mass transfer enhancement, E_p, by suspended particles or electrolyte in the slurry, is defined as

$$E_p = \frac{(k_l a_l)_p}{(k_l a_l)_0} \tag{17}$$

The physical mass transfer coefficient $(k_l a_l)_p$ changes to $(k_l a_l)_r$ in the presence of reaction. The reaction enhancement factor, E_r, and the total enhancement factor, E_t, are defined as

$$E_t = \frac{(k_l a_l)_r}{(k_l a_l)_0}, \qquad E_r = \frac{(k_l a_l)_r}{(k_l a_l)_p}, \qquad E_t = E_r E_p \tag{18}$$

All the effects of enhancement due to mechanisms 1–4 are incorporated in the total enhancement factor, E_t.

3. Results and discussion

3.1. Aqueous phase: physical enhancement

The stirring rate, the electrolyte concentration, and the particle concentration were varied and the mass transfer enhancement factor is separately presented for electrolyte solutions, for particle slurries, and for their combinations.

3.1.1. Electrolyte

The influence of glucose and a combination of glucose–electrolyte on mass transfer enhancement, is presented in Fig. 3a. The E_p values for 0.4 M G–0.1 M E are smaller than for 0.1 M G–0.4 M E (based on starting concentration of 0.5 M glucose) at all mixing intensities. For glucose–distilled

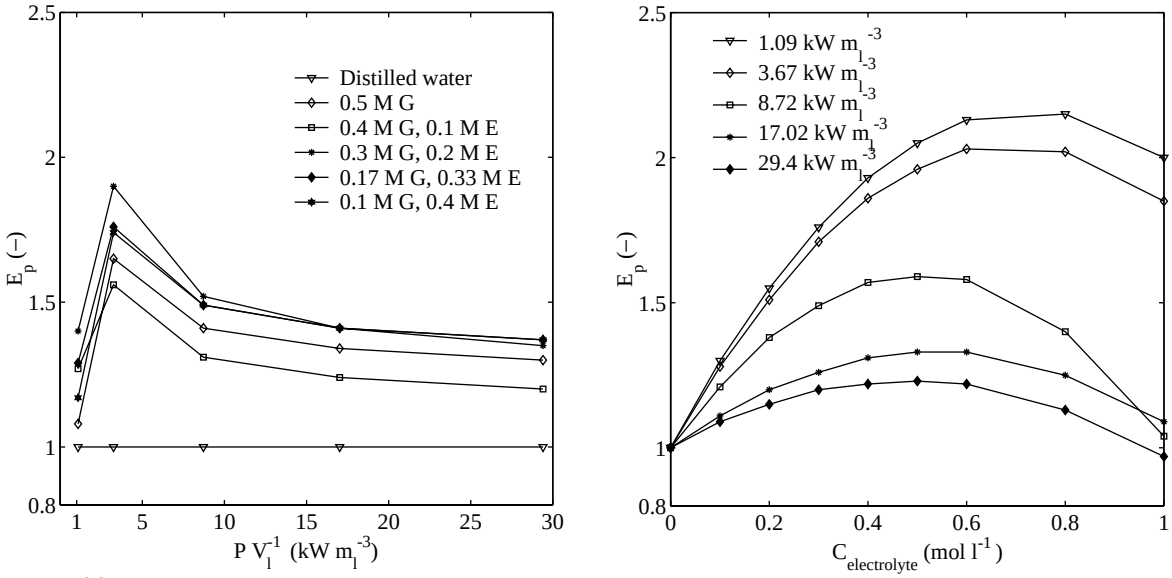

(a) Glucose solution, O_2 gas, electrolyte (b) Distilled water, O_2 gas, electrolyte

Fig. 3. Effect of electrolyte on gas–liquid mass transfer measured using pressure-step method with distilled water at 1 bar and 323 K.

water only, the enhancement factor is around 1.4 and in combination with glucose-electrolyte–distilled water, it is same. The influence of glucose on surface tension is found to be negligible. Higher enhancement due to glucose is regarded as resulting from the higher viscosity of the solution. The residence time of a gas bubble in the system is linearly proportional to viscosity and coalescence inhibition increases with viscosity. Hence, the gas–liquid interfacial area (a_l) increases. The difference between glucose–electrolyte (Fig. 3a) and distilled water–electrolyte (Fig. 3b) at all mixing intensities is negligible (within 90% confidence). Therefore, the additional influence of glucose to distilled water–electrolyte solution is negligible and the study of the combination of particles and electrolyte is done using distilled water. The following interpretations can be made from Fig. 3: (i) at low mixing intensity, addition of electrolyte contributes to an additional enhancement factor of 1.8 (Fig. 3a); (ii) the enhancement factor increases with electrolyte concentration and attains a maximum value of 2.1 at 0.6 M electrolyte solution (Fig. 3b), beyond which it decreases; (iii) the enhancement factor decreases with increasing mixing intensity and is 1.4 at high mixing intensity (Fig. 3a). The presence of an electrolyte changes the surface tension which is a measure for the stability of the G–L interface. The surface tension for distilled water is 74.7 mN m^{-1} and decreases to 58 ± 3 mN m^{-1} with increasing electrolyte concentration up to 0.3–04 M, beyond which it becomes independent of electrolyte concentration. A lower surface tension leads to a less stable G–L interface and thus to a smaller average bubble size. On the other hand, a decreasing surface tension, also decreases k_l, since it reduces the rate of surface renewal [16]. The viscosity of distilled water is 0.578 mPa s and of 0.33 M electrolyte is 0.628 mPa s at 323 K. At a very high concentration of electrolyte (>0.6–1 M), although the surface tension does not decrease further, the viscosity of the liquid is increased strongly (1.12 mPa s for 1 M electrolyte at 323 K). Since the molecular diffusivity and turbulent diffusivity are inversely proportional to the viscosity [38], the increase in viscosity beyond 0.6 M electrolyte reduces the value of $k_l a_1$. The effect of electrolyte at high mixing intensity is not very pronounced. It is concluded that mechanism 3 (coalescence inhibition) is the only governing mechanism both at low and high mixing intensities.

3.1.2. Particles

From Fig. 4a, no dependency is seen between the volumetric mass transfer coefficient and the carbon concentration. The maximum value of E_p at very low mixing intensity of 1 kW m$_l^{-3}$ is around 1.5. Beyond a mixing intensity of 15 kW m$_l^{-3}$, the value is around unity. The values below 1 may be attributed to turbulence inhibition effect. The difference between pure distilled water and silica particles is small (enhancement factor of 1.2) at all mixing intensities as shown in Fig. 4d. For 1 g l^{-1} silica and carbon, an opposite trend is observed at the lowest mixing intensity. This is attributed to the fact, that dense silica particles are not distributed uniformly at low mixing intensity and collisions with the G–L boundary layer are ineffective, whereas carbon particles adhere readily to the interface at low mixing intensity. For particle concentrations below 0.6 vol.% (approximately 3 g l^{-1}), the small lyophobic particles may cover the bubble surface, preventing coalescence of the bubbles. Thus smaller bubbles with a lower rise velocity are present with a larger interfacial area. However, adding more particles (typically >0.6 vol.%) will not further increase

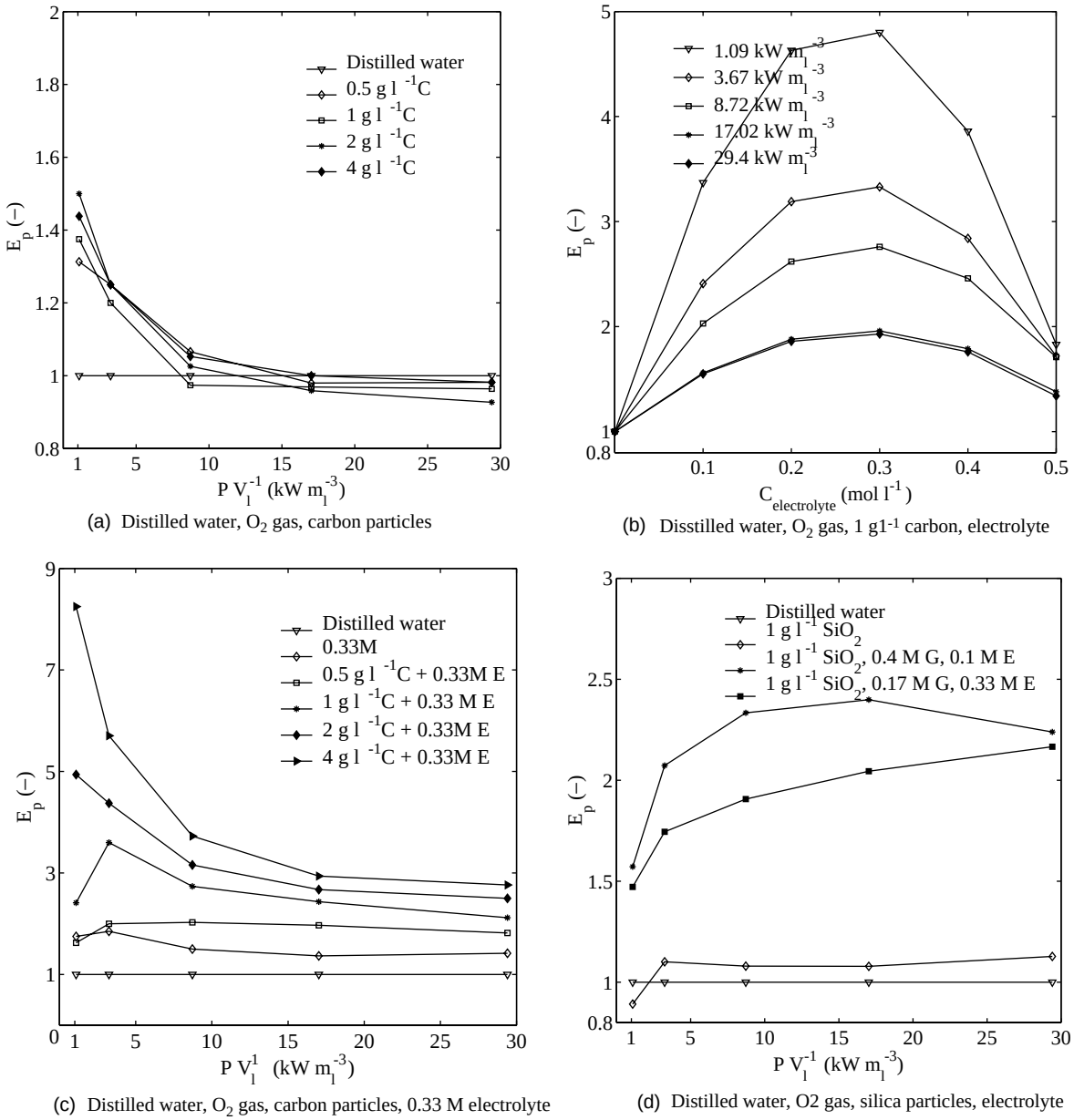

(a) Distilled water, O_2 gas, carbon particles

(b) Disstilled water, O_2 gas, 1 g1-1 carbon, electrolyte

(c) Distilled water, O_2 gas, carbon particles, 0.33 M electrolyte

(d) Distilled water, O2 gas, silica particles, electrolyte

Fig. 4. Effect of glucose concentration, carbon particle concentration, combinations of carbon or silica particles with electrolyte on gas–liquid mass transfer measured using pressure step method with distilled water at 1 bar and 323 K.

the interfacial area. The bubble surface is then already sufficiently covered for a maximum coalescence inhibition. Based on above mentioned observations, mechanism 1 is the likely one to account for the increased rate of mass transfer at low stirring rates. It is expected that the surface tension is hardly influenced by the presence of carbon or silica particles. Mechanism 2 is not relevant since the observed enhancement decreases with stirring rate and does not increase proportionally to particle concentration. There is no dependency on carbon concentration beyond a mixing intensity of $10\,\mathrm{kW\,m_l^{-3}}$ where the enhancement factor is nearly 1 since mixing forces are much higher than particle induced forces at the G–L boundary layer. At high mixing intensity, neither mechanism 1 (additional refreshment of liquid at the G–L boundary layer), nor mechanism 3 (coalescence inhibition) contribute to an enhanced mass transfer.

3.1.3. Particles and electrolyte

Since during oxidation of glucose, both electrolyte and particles (carbon or silica, Pd–Bi/C or Pd–Bi/SiO_2) are present, it is relevant to study the combined effect. Comparison of Fig. 4b with Fig. 3b, shows that, addition of $1\,\mathrm{g\,l^{-1}}$ carbon to electrolyte solutions, has a very pronounced effect on the mass transfer rate. The value of E_p increases with electrolyte concentration and attains a maximum between 0.3 and 0.4 M, beyond which it decreases. Enhancement

factors are significantly higher compared to the case of pure electrolyte, and attain a maximum of 4.80 at 0.3 M electrolyte concentration at low mixing intensity. Based on such a pronounced effect of the combination of particles and electrolyte, the concentration of carbon particles was varied at an electrolyte concentration of 0.33 M (Fig. 4c). The results for silica particles are shown in Fig. 4d. Clearly, the combination of particles and electrolyte significantly increases the enhancement factor.

At low mixing intensity, a maximum value of 8.2 for $4\,g\,l^{-1}$ carbon–0.33 M electrolyte slurry and a maximum value of 1.6 for $1\,g\,l^{-1}$ silica–0.1 M electrolyte–0.4 M glucose slurry is obtained. The accuracy of the data is within the ±5% error. It is suggested that: (i) addition of electrolyte, active carbon, or silica particles together stabilises the bubbles. This stabilisation is the result of the formation of a layer of particles, and/or particles with adsorbed electrolyte around the gas bubble, which hinders bubble coalescence as discussed in Section 1 for mechanism 3; (ii) particles with adsorbed electrolyte have a higher tendency for PBA [39]. Also, sedimentation experiments show that particle agglomeration is delayed. Carbon particles in water readily form agglomerates and settle down (settling time ≈5 min), whereas electrolyte stabilises the slurry (settling time ≈30 min). An increase in electrolyte concentration reduces the interaction potential energy between the particle and bubble, as well as the critical film rupture thickness. Thus, the film drainage rate increases between particle and bubble [40]; (iii) a larger fraction of carbon particles, having nearly the same density as the liquid, adheres to the G–L interface and therefore local boundary layer turbulence is more vigorous. It increases k_l by refreshment of liquid. For the heavier, non-adhering silica particles, increase in k_l is only by collisions with the G–L interface; (iv) when the density or the viscosity of the liquid-slurry around the bubble is significantly increased, the rise velocity of the bubble will be lowered at low stirring rates, which results in a higher gas hold-up. Thus, it is suggested that both mechanisms 1 and 3 play a role at low mixing intensity.

At high mixing intensity, the enhancement factor decreases in case of the carbon slurry (Fig. 4c) but increases for the silica slurry (Fig. 4d). When comparing Figs. 3a and 4a at the highest mixing intensity, a maximum enhancement factor of 1.4 is found for the case of electrolyte. This value is much lower than the combination of carbon particles and electrolyte at the highest mixing intensity (maximum value of 3 from Fig. 4c). Apparently, even at high mixing intensity, carbon particles in electrolyte stabilises bubbles, in contrast with carbon particles in pure water. The enhancement factor increases with the carbon concentration in the presence of electrolyte. For the case of silica particles, the difference in the enhancement factor between pure distilled water and added silica particles is small (value of 1.2). For the combination of silica particles and electrolyte, a maximum enhancement factor of 2.4 for 0.1 M electrolyte, and 2.2 for 0.33 M electrolyte is attained. The enhancement factor clearly increases with mixing intensity up to $17\,kW\,m_l^{-3}$ for the silica–electrolyte–glucose slurry, after which it reaches a plateau. The difference between solid and liquid density is an important parameter in relation to k_la_l. The greater inertia of the heavier silica particles, creates stronger collisions at the G–L interface at high shear rate and thereby affects the value of k_l [41]. Thus, mechanisms 1 and 3 act concurrently for silica particles at high mixing intensity.

3.2. Organic phase: physical enhancement

The stirring rate and the carbon or silica concentrations are varied and the initial, specific rate of absorption of hydrogen in the AMS–cumene liquid, is determined from dynamic gas absorption experiments. For AMS hydrogenation, the product cumene does not change the surface tension of the liquid nor the viscosity. From Fig. 5, it is noticeable that the enhancement factor of hydrogen absorption in the presence of carbon or silica particles in AMS–cumene slurry is significantly lower than the enhancement factor of oxygen absorption in distilled water–electrolyte slurry. But, the enhancement factor at high mixing intensity in the AMS–cumene slurry with carbon or silica particles, is higher than in the distilled water slurry without electrolyte. The results for hydrogen absorption in AMS–carbon slurry and AMS–silica slurry shown in Fig. 5, are more or less similar. Thus probably, silica is not lyophobic enough to adhere to the G–L interface or the lyophobicity/lyophilicity of the particles is less important in organic liquids.

At low mixing intensity, the maximum physical enhancement factor is 1.7 in the AMS–silica slurry and is 1.4 in the AMS–carbon slurry. As illustrated in Fig. 5, the enhancement decreases at higher particle concentrations after which it levels off. There is a critical particle concentration of $1\,g\,l^{-1}$ observed for both the silica and the carbon slurries, beyond which no further increase of the enhancement factor is found. This observation is in agreement with experimental observations for other gas-activated carbon slurry systems [5,42] and our results in Section 3.1 without electrolyte. The enhancement factor decreases at high mixing intensity. Contrary to distilled water, no difference between carbon and silica behaviour is observed and hence the collision effect is absent. It is concluded that mechanism 1 is operative and adhering particles increase k_l, due to increased refreshment of the G–L boundary layer.

At high mixing intensity, the maximum physical enhancement factor is 1.3–1.4 for both carbon and silica slurries. The influence of particles on G–L mass transfer decreases, and the same explanation holds as described for aqueous slurry (mechanisms 1 and 3 as an additive effect). Mechanism 2 is not present due to: (i) the same behaviour of carbon and silica particles which may be due to the fact that the particle size is one order of magnitude higher than the thickness of particle free G–L boundary layer; (ii) the difference in measured values of partition coefficient for H_2–silica slurry

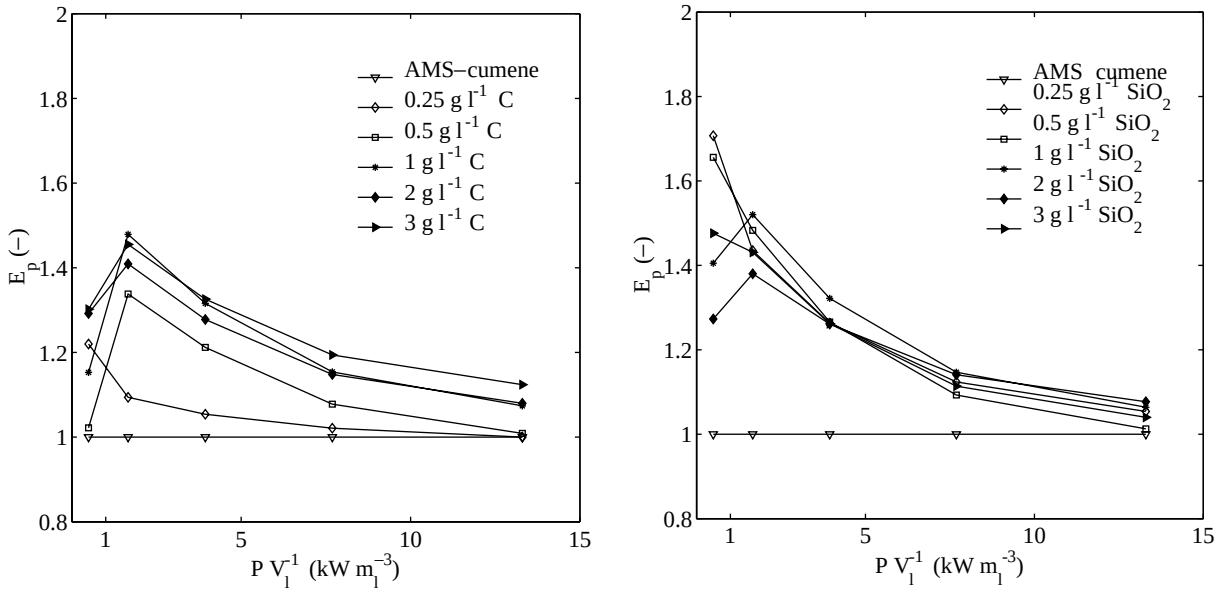

(a) AMS-cumene, H_2 gas, carbon particles (b) AMS-cumene, H_2 gas, silica particles

Fig. 5. Effect of carbon and silica particles on gas–liquid mass transfer measured using dynamic gas absorption with organic AMS–cumene mixture (80:20 vol.%) at 1 bar and 303 K.

($m = 6.1 \pm 5\%$) and H_2–carbon slurry ($m = 40 \pm 10\%$) is too low, where m must be of the order of 400, to have mechanism 2 as contributing factor [19]; (iii) the enhancement factor decreases with mixing intensity and no particle concentration dependency is found. It is concluded that mechanism 3 (coalescence inhibition) is operative at high mixing intensity, but has a limited effect.

3.3. Aqueous phase: reaction enhancement

Pseudo-steady-state experiments were performed with reaction in the GIR and the results are shown in Fig. 6. The measured liquid phase concentration of oxygen is zero for all glucose oxidation experiments, due to the high activity of the catalyst. As illustrated in Fig. 1, the main route for

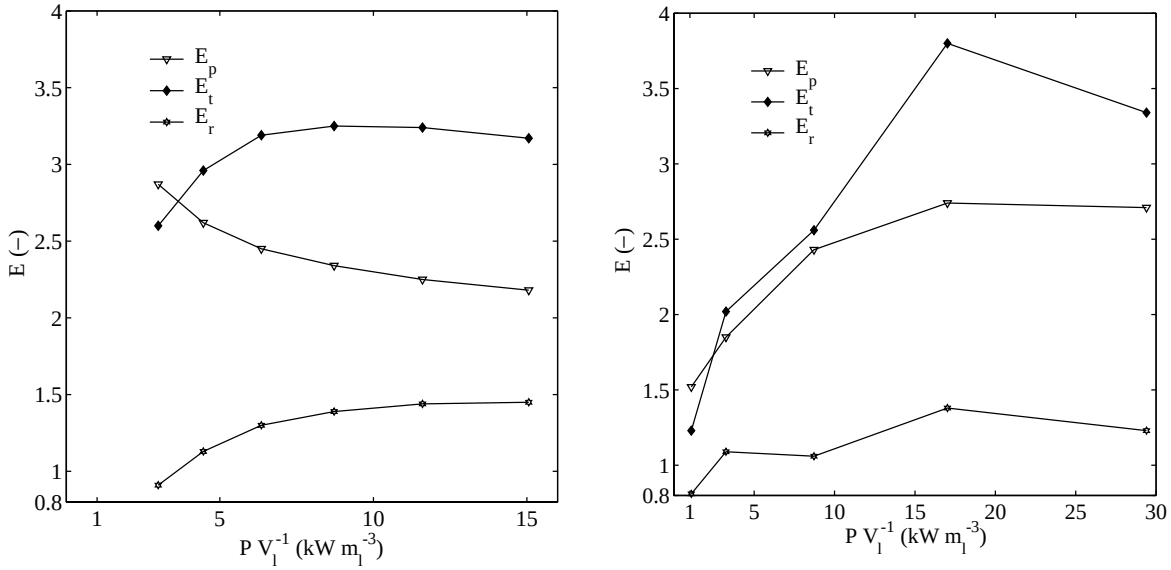

(a) 1 g 1^{-1} 3% Pd/C (b) 1 g 1^{-1} 3% Pd/SiO_2

Fig. 6. Comparison of physical and chemical reaction enhancement measured in the GIR for aqueous glucose oxidation as a function of impeller speed: $P = 1.05$ bar, $T = 323$ K, pH 9, Pd/Bi = 5 mol/mol, initial $C_{gluc} = 500$ mol/m^3, $p_{O_2} = 0.2$ bar, conversion = 0–60%. E_p reference is 1 g $l^{-1} + 0.1$ M electrolyte.

oxygen transport is directly from the gas phase to the liquid filled wetted catalyst particle [36]. Also, mechanism 4 due to PBA might be operative. The calculation of the reaction enhancement factor is complicated due to the following reasons: (i) the reaction product sodium gluconate itself is an electrolyte and hence the concentration of electrolyte and glucose changes in time, thereby changing the catalyst potential. We have shown its importance in Section 3.1 and it is also clear from Fig. 4; (ii) the adhesion behaviour for the catalyst particles may be different (see ΔH_i from Table 2) and can also change during reaction. The catalyst is more lyophilic and hence PBA is expected to be less, thereby lowering the physical enhancement factor; (iii) the influence of the catalyst promoter Bi and noble metal Pd on the volumetric G–L mass transfer coefficient is unknown. Due to all these uncertainties, it is difficult to find a proper reference value for E_p. However, we assumed a reference of $1\,g\,l^{-1}$ carbon or silica with 0.1 M electrolyte and the calculated enhancement factor is presented in Figs. 6a and b. For the Pd/SiO_2 particles, the value of $(k_l a_l)_r$ is calculated from Eq. (11) under reactive conditions. The reaction enhancement factor is calculated with this value because full mass transfer limiting conditions do not apply yet. Only at a catalyst concentration above $1\,g\,l^{-1}$, the measured bulk liquid

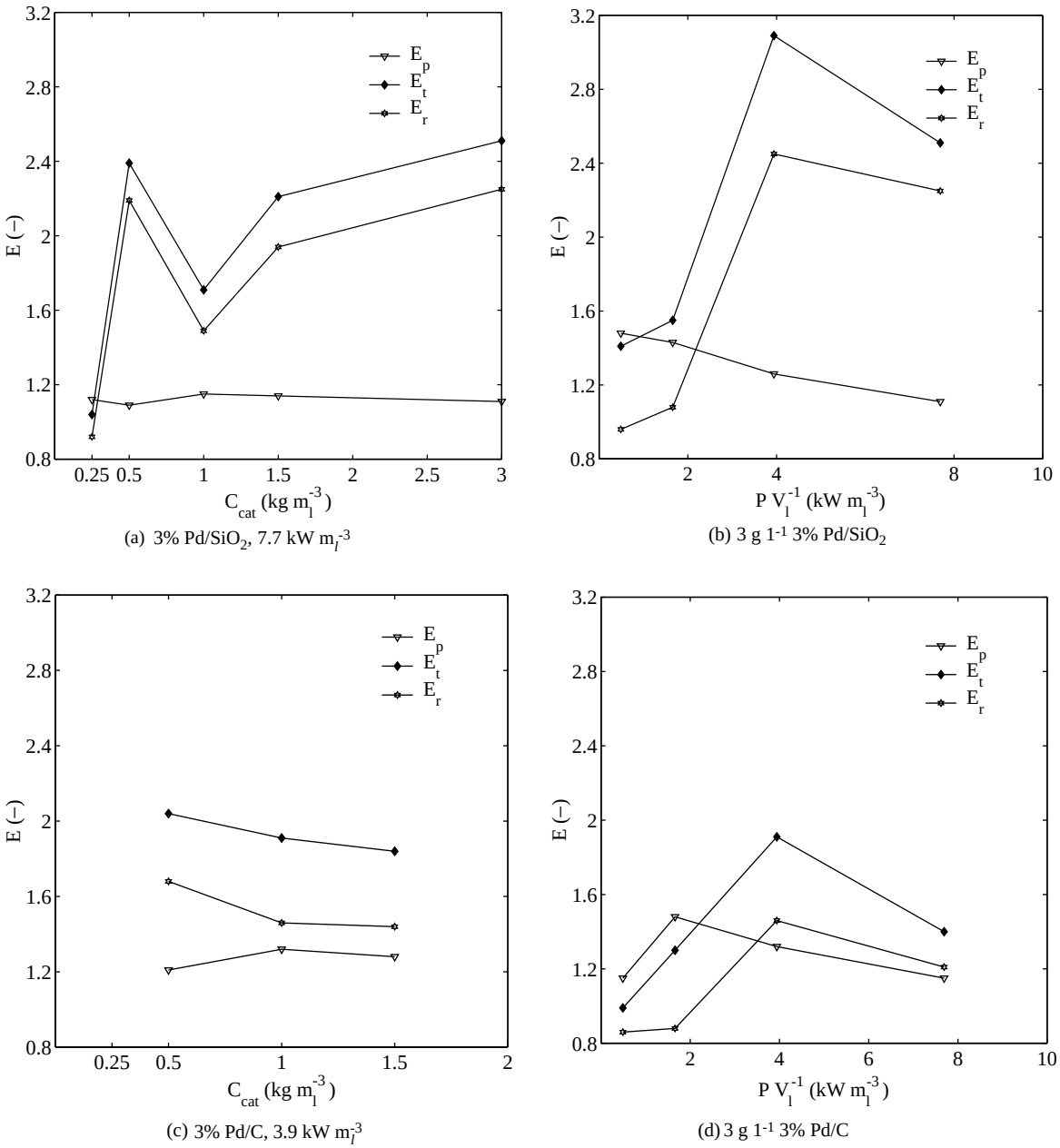

(a) 3% Pd/SiO_2, 7.7 kW m_l^{-3}

(b) 3 g l^{-1} 3% Pd/SiO_2

(c) 3% Pd/C, 3.9 kW m_l^{-3}

(d) 3 g l^{-1} 3% Pd/C

Fig. 7. Comparison of physical and chemical reaction enhancement measured in the GIR for organic AMS hydrogenation as a function of catalyst loading and impeller speed: $P = 1$ bar, $T = 303$ K, pure H_2 gas; effectiveness factor η is 0.4 (3% Pd/SiO_2) and 0.61 (3% Pd/C).

oxygen concentration is zero. It is observed that the reaction enhancement (E_r by mechanism 4) in the glucose–carbon slurry is higher than the glucose–silica slurry. This may be due to the fact that eggshell carbon catalyst has higher activity than uniform silica catalyst [36]. The value of E_r for carbon and silica catalyst increases with stirring rate (range of 1.2–1.4 from Fig. 6a and b). Although the physical and reaction enhancement for silica catalyst increases with stirring rate, an opposite trend is observed for carbon catalyst as explained earlier. The maximum total enhancement observed is 3.2 for carbon catalyst and 3.5 for silica catalyst. In conclusion, there is a limited contribution of reaction enhancement to oxygen mass transfer in the presence of carbon or silica supported catalyst. And, the overwhelming physical enhancement obscures this effect.

3.4. Organic phase: reaction enhancement

Pseudo-steady-state experiments were performed with AMS hydrogenation in the GIR of which the results are shown in Fig. 7. With the literature values for mk_r, reaction enhancement factors less than unity are obtained. This cannot be explained by: (i) experimental errors due to comparison of dynamic gas absorption method and pseudo-steady-state absorption method [43]; or (ii) incorrect use of Eq. (11) to represent the effect of PBA, as is considered in [36]. Since $E_r \geq 1$, a sensitivity analysis for the value of mk_r is done for both 3% Pd/C and 3% Pd/SiO_2 catalyst. It has been found that the value of mk_r for the case of silica particles is at least 3.13 (i.e., $m = 1$), but for carbon particles, mk_r is 25 (i.e., $m = 8$) to get all $E_r \geq 1$. This later value is also reported by Tinge and Drinkenburg [11] for the adsorption of hydrogen gas on carbon particles. From Fig. 7a, a maximum reaction enhancement factor of 2.4 in the AMS–Pd/SiO_2 slurry is observed at all catalyst loadings where the physical enhancement factor equals 1.1. In Fig. 7b, the reaction enhancement increases with stirring rate in the case of AMS–Pd/SiO_2 slurry. It appears to flatten out or even decrease after $8\,kW\,m_l^{-3}$ giving a maximum reaction enhancement factor of 3.0 at $4\,kW\,m_l^{-3}$. For 3% Pd/C slurry, a reaction enhancement factor in the range of 1–1.6 is found, see Fig. 7c and d. It is not very much dependent on the catalyst concentration nor on the mixing intensity. Concluding, the relative lyophobicity/lyophilicity of carbon and silica particles is especially important concerning mechanism 4 (reaction enhancement) in organic slurries. However, it is insignificant for the physical mechanisms discussed in Section 3.2.

4. Conclusions

It has been shown that by combining the results of experiments with two different catalyst supports, i.e., carbon and silica particles, along with an aqueous electrolyte solution and organic liquid, using an oxidation as well as hydrogenation reaction, it is possible to identify the operating mechanisms of G–L mass transfer enhancement. We have found that:

(1) For an AMS–H_2 slurry, physical enhancement factors up to 1.7 for silica particles and 1.4 for carbon particles are observed. For a glucose–O_2 slurry, physical enhancement factors up to 1.4 for carbon particles and 1.1 for silica particles are observed. For aqueous liquids, carbon particles adhere to the G–L interface and induce local turbulence. Collisions of silica particles refresh the G–L interface. Both effects enhance the rate of mass transfer (mechanism 1). For organic liquids, carbon and silica particles equally refresh the G–L interface at low mixing intensities only (mechanism 1). This effect levels off at high particle concentration.

(2) Enhancement of mass transfer by shuttling of particles between the G–L interface and the bulk liquid (mechanism 2) is insignificant since it is found that (i) the enhancement factor decreases with stirring rate and (ii) reaches a plateau after some critical particle concentration.

(3) Enhancement factors up to 3.5 for distilled water–0.33 M electrolyte–carbon and 2.1 for distilled water–0.33 M electrolyte–silica particles, are observed with a particle loading of $1\,g\,l^{-1}$ at $\sim 2\,kW\,m_l^{-3}$. The highest value of enhancement is 8.2 for distilled water–$4\,g\,l^{-1}$ carbon–0.33 M electrolyte at $\sim 1\,kW\,m_l^{-3}$. For silica particles, the enhancement factor increases with mixing intensity to a maximum value of 2.4 at $15\,kW\,m_l^{-3}$ and then levels off. Maximum enhancement factor of 1.4 (only electrolyte), 1.0 (only carbon), and 3.0 (their combination) prevails at high mixing intensities (mechanism 3) along with mechanism 1 as a concurrent effect. Whereas for AMS–cumene slurry, maximum physical enhancement factors of 1.3 (carbon particles) and 1.2 (silica particles) at high mixing intensity (mechanism 3) are obtained.

(4) The rate of mass transfer in aqueous slurry is very pronounced when in combination with electrolyte and carbon or silica particles, which is attributed to an increase in the specific gas–liquid interfacial area a_l (mechanism 3). The addition of both solid particles and electrolyte together changes the local electrostatic potential on solid particles or ionic bubbles which in turn promotes particle–bubble adhesion, thereby inhibiting bubble coalescence (stabilising effect). For organic liquid, at high mixing intensity, mechanism 3 is operative but has a limited effect.

(5) The mass transfer coefficient in the presence of reaction is higher (mechanism 4) as compared to physical mass transfer in the presence of solids. The reaction enhancement for glucose oxidation is complicated due to the uncertainty in the reference value for the physical enhancement. The reaction enhancement is obscured due to an overwhelming physical enhancement in the

glucose–carbon–electrolyte slurry. The reaction enhancement factor increases with mixing intensity up to a certain value, after which it becomes constant. The reaction enhancement factor for glucose–carbon slurry (1.3–1.5) is higher than for glucose–silica slurry (1.0–1.3). And, for the AMS–carbon slurry (1.2–1.4) is less than the AMS–silica slurry (2.0–2.4). Thus, the relative behaviour of carbon and silica catalyst in organic phase is the reverse of the behaviour in an aqueous phase.

(6) Lyophobicity/lyophilicity of the carbon/silica catalyst particles determines the interaction with the G–L interface. In aqueous glucose slurry, physical enhancement (mechanisms 1 and 3) and reaction enhancement (mechanism 4) are observed. In organic AMS–cumene slurry, lyophobicity/lyophilicity affects reaction enhancement only.

Acknowledgements

The authors gratefully acknowledge the Dutch Technology Foundation STW (EPC. project 5239), Akzo Nobel, DSM Research B.V., and Shell Global Solutions for their financial support and Engelhard B.V. and Promeks ASA for supplying the catalyst samples. Experimental assistance of W.P.T. Groenland and S. Ophof is appreciated.

References

[1] K.C. Ruthiya, B.F.M. Kuster, J.C. Schouten, Gas–liquid mass transfer enhancement in a surface aeration stirred slurry reactor, Can. J. Chem. Eng. 81 (2003) 632–639.
[2] M.M. Sharma, R.A. Mashelkar, Absorption with reaction in bubble columns, Int. Chem. E. Symp. Ser. 28 (1968) 10–21.
[3] Y.Y. Lee, G.T. Tsao, Oxygen absorption in glucose solution, Chem. Eng. Sci. 27 (1972) 1601–1608.
[4] R.L. Kars, R.J. Best, A.A.H. Drinkenburg, The sorption of propane in slurries of active carbon in water, Chem. Eng. J. 17 (1979) 201–210.
[5] E. Alper, B. Wichtendahl, W.-D. Deckwer, Gas absorption mechanism in catalytic slurry reactors, Chem. Eng. Sci. 35 (1980) 217–222.
[6] P.V. Danckwerts, Gas–Liquid Reactions, McGraw-Hill, New York, 1970.
[7] R.D. Holstvoogd, W.P.M van Swaaij, L.L. van Dierendonck, The adsorption of gases in aqueous activated carbon slurries enhanced by adsorbing or catalyst particles, Chem. Eng. Sci. 43 (8) (1988) 2181–2187.
[8] D. Lindner, M. Werner, A. Schumpe, Hydrogen transfer in slurries of carbon supported catalysts (HPO) process, AIChE J. 34 (10) (1988) 1691–1697.
[9] O.J. Wimmers, J.M.H. Fortuin, The use of adhesion of catalyst particles to gas bubble to achieve enhancement of gas absorption in slurry reactor, Part II, Chem. Eng. Sci. 43 (1988) 313–319.
[10] H. Vinke, P.J. Hamersma, J.M.H. Fortuin, Particle-to-bubble adhesion in gas–liquid–solid slurries, AIChE J. 37 (12) (1991) 1801–1809.
[11] J.T. Tinge, A.A.H. Drinkenburg, The enhancement of the physical absorption of gases in aqueous activated carbon slurries, Chem. Eng. Sci. 50 (6) (1995) 937–942.
[12] M. van der Zon, P.J. Hamersma, E.K. Poels, A. Bliek, Gas–solid adhesion and solid–solid agglomeration of carbon-supported catalysts in 3-phase slurry reactors, Catal. Today 48 (1–4) (1999) 131–138.
[13] H. Vinke, P.J. Hamersma, J.M.H. Fortuin, Enhancement of the gas-absorption rate in agitated slurry reactors by gas-adsorbing particles adhering to gas-bubbles, Chem. Eng. Sci. 48 (12) (1993) 2197–2210.
[14] J.H.J. Kluytmans, B.G.M. van Wachem, B.F.M. Kuster, J.C. Schouten, Mass transfer in sparged and stirred reactors: influence of carbon particles and electrolyte, Chem. Eng. Sci., in press.
[15] S.P. Godbole, A. Schumpe, Y.T. Shah, The effect of solid wettability on gas–liquid mass transfer in a slurry bubble column, Chem. Eng. Sci. 45 (1990) 3593–3595.
[16] A.K. Suresh, T. Sridhar, O.E. Potter, Mass transfer and solubility in autocatalytic oxidation of cyclohexane, AIChE J. 34 (1988) 55–68.
[17] A.A.C.M. Beenackers, W.P.M. van Swaaij, Mass-transfer in gas–liquid slurry reactors: review article, Chem. Eng. Sci. 48 (18) (1993) 3109–3139.
[18] G. Quicker, E. Alper, W.-D. Deckwer, Effect of fine activated carbon particles on the rate of CO_2 absorption, AIChE J. 33 (1987) 871–875.
[19] J.F. Demmink, A. Mehra, A.A.C.M. Beenackers, Gas absorption in the presence of particles showing interfacial affinity: case of fine sulfur precipitates, Chem. Eng. Sci. 53 (16) (1998) 2885–2902.
[20] A. Schumpe, A.K. Saxena, L.K. Fang, Gas/liquid mass transfer in a slurry bubble column, Chem. Eng. Sci. 42 (7) (1987) 1787–1796.
[21] G. Marrucci, A theory of coalescence, Chem. Eng. Sci. 24 (1969) 975–985.
[22] M.J. Prince, H.W. Blanch, Transition electrolyte concentrations for bubble coalescence, AIChE J. 36 (9) (1990) 1425–1429.
[23] M. Jamialahmadi, H. Muller-Steinhagen, Effect of solid particles on gas hold-up in bubble columns, Can. J. Chem. Eng. 69 (1991) 390–393.
[24] G. Quicker, E. Alper, W.-D. Deckwer, Gas absorption rates in a stirred cell with plane interface in the presence of fine particles, Can. J. Chem. Eng. 67 (1989) 32–38.
[25] J.H. Lee, N.R. Foster, Measurement of gas–liquid mass transfer in multiphase reactors, Appl. Catal. 63 (1990) 1–36.
[26] M.V. Dagaonkar, H.J. Heeres, A.A.C.M. Beenackers, V.G. Pangarkar, Investigation of enhanced gas absorption by adsorptive bucky balls in a multiphase slurry reactor in the presence and absence of ultrasound, Ind. Eng. Chem. Res. 41 (2002) 1496–1503.
[27] V. Linek, P. Benes, J. Sinkule, T. Moucha, Non ideal pressure step method for k_la_l measurement, Chem. Eng. Sci. 48 (1993) 1593–1599.
[28] H.M. Letzel, A. Stankiewicz, Gas hold-up and mass-transfer in gas-lift reactors operated at elevated pressures, Chem. Eng. Sci. 54 (21) (1999) 5153–5157.
[29] M. Besson, F. Lahmer, P. Gallezot, Catalytic oxidation of glucose on bismuth-promoted palladium catalysts, J. Catal. 152 (1995) 116–121.
[30] S.-Y. Chen, J.M. Smith, B.J. Mccoy, Effect of hydrogenation catalyst activity on adsorption and surface reaction rates, Chem. Eng. Sci. 42 (2) (1987) 293–306.
[31] H.S. Fogler, Elements of Chemical Reaction Engineering, 3rd ed., Prentice-Hall, Engelwood Cliffs, NJ, 1999.
[32] K. Kawakami, S. Ura, K. Kusunoki, The effectiveness factor of a catalyst pellet in the liquid phase hydrogenation of styrene, J. Chem. Eng. Jpn. 9 (5) (1976) 392–396.
[33] I. Mazzarino, A comparative-study of sandwich cross-flow and random catalytic packings for multiphase chemical reactors, Chem. Eng. Sci. 54 (15–16) (1999) 3677–3682.
[34] S.B. Satterfield, Y.H. Ma, T.K. Sherwood, The effectiveness factor in a liquid filled porous catalysts, Int. Chem. Eng. Symp. Ser. 28 (1968) 22–29.
[35] M. Herskowitz, S. Mosseri, Global rates of reaction in trickle bed reactors, Ind. Eng. Chem. Fundam. 22 (1974) 4–6.
[36] K.C. Ruthiya, J. van der Schaaf, B.F.M. Kuster, J.C. Schouten, Modelling catalytic reaction rate at gas–liquid interface: influence of metal content, metal distribution and particle diameter, AIChE J. (2003), submitted.

[37] Y. Sano, N. Yamaguchi, T. Adachi, Mass transfer coefficients for suspended particles in agitated vessels and bubble columns, J. Chem. Eng. Jpn. 7 (1974) 255–261.
[38] C.R. Wilke, P. Chang, Correlations of diffusion coefficients in dilute solutions, AIChE J. 1 (1955) 264–270.
[39] P.C. Hiemenz, Principles of Colloid and Surface Chemistry, 2nd ed., Marcel Dekker, New York, 1986.
[40] J. Ralston, D. Fornasiero, R. Hayes, Bubble–particle attachment and detachment in flotation, Int. J. Miner. Process. 56 (1999) 133–164.
[41] G.E.H. Joosten, J.G.M. Schilder, J.J. Janssen, The influence of suspended solid material on the gas–liquid mass transfer in stirred slurry reactors, Chem. Eng. Sci. 32 (1977) 563–566.
[42] E. Alper, S. Ozturk, Effect of fine solid particles on gas–liquid mass transfer rate in a slurry reactor, Chem. Eng. Commun. 46 (1986) 147–158.
[43] V. Linek, P. Benes, V. Vacek, F. Hovorka, Analysis of differences in $k_l a$ values determined by steady-state and dynamic methods in stirred tanks, Chem. Eng. J. 25 (1982) 77–88.
[44] R.C. Bates, P.L. Fondy, R.R. Corpstein, An examination of some geometric parameters of impeller power, Ind. Eng. Chem. Proc. Des. Dev. 3 (1963) 310.
[45] E.F. Stefoglo, Experimental study of the hydrogenation process in gas–liquid reactors on a suspended catalyst, Chem. Eng. Commun. 4 (1986) 327–337.
[46] R.H. Perry, D.W. Green, J.O. Maloney, Perry's Chemical Engineers Handbook, 7th ed., McGraw-Hill, New York, 1997.
[47] L. Bartovska, M. Siskova, J. Rumplik, Surface tension–viscosity correlation in aqueous solutions of saccharides, Sb. Vys. Sk. Chem. Technol. Praze, N: Fyz. Chem. N10 (1990) 275–299.